Dynamic-State-Estimation-Based Cyber Attack Detection for Inverter-Based Resources

Avinash Kumar, Yuzhang Lin, Heqing Huang
Department of ECE
University of Massachusetts, Lowell
{avinash_kumar,yuzhang_lin}@uml.edu,
heqing_huang@student.uml.edu

Xiaonan Lu
School of Engineering Technology
Purdue University
lu998@purdue.edu

Yue Zhao
Department of ECE
Stony Brook University
yue.zhao.2@stonybrook.edu

2023 IEEE Power & Energy Society General Meeting (PESGM) | 978-1-6654-6441-3/23/$31.00 ©2023 IEEE | DOI: 10.1109/PESGM52003.2023.10252357

***Abstract*—The cyber security of Inverter Based Resources (IBRs) has received increasing attention in recent years. In this paper, a cyber attack detection method is proposed based on dynamic state estimation for IBRs. The state-space models of the physical inverter system and the digital controller are separately derived and then coupled by the data flows in between, i.e., measurement signals and control signals. Based on Kalman Filtering (KF), two dual dynamic state estimators are developed for tracking the cyber and physical state variables, respectively. By checking the model-data consistency of both the physical and cyber layers via hypothesis testing, the proposed method features the capability of distinguishing between false data in measurement signals and in control signals. Simulation results in an IEEE 13 node test feeder demonstrate the effectiveness of the proposed method.**

***Index Terms*—Dynamic state estimation, Inverter based resources, Kalman filter, Cyber security, Event detection.**

I. Introduction

The fast-acting control of IBRs and the absence of a rotational part especially in Solar Photovoltaic (SPV) and battery energy storage systems are changing the dynamics of the system during disturbances. While the growing integration of IBRs leads to significant economic and environmental benefits [1], [2], the security, reliability, and resiliency of IBRs has become one major concern. Unlike conventional synchronous generators, the dynamics of IBRs are heavily determined by their digital controllers, which interact with the physical inverter system via fast measurement signals and control signals. The exchange of information between the cyber layer and the physical layer can easily be exposed to attackers, who can inject false data to compromise the performance of IBRs [3], [4]. Furthermore, IBRs are only equipped with a few sensors at the terminals, and the internal operating conditions of both the digital controller and the physical inverter system are not directly monitored. Therefore, state and security monitoring of IBRs will play important role in the operations and control of IBR-integrated power grids.

To track the states of grid components, dynamic state estimation methods have been widely studied and used in conventional bulk power grids with synchronous generators [5]. Different variants of dynamic state estimation methods are developed based on the consideration of various applications, dynamics components, time scales, and computation efficiency requirements (see [6]–[8]). A detailed review of dynamic state estimation techniques and applications can be found in [5].

Despite significant progress in the research of dynamic state estimation for synchronous generators, few papers on dynamic state estimation for IBRs have been reported. The stability of three loop control of IBR using state variable is developed in [9]. The unscented KF-based dynamic state estimation of a doubly fed induction generator is proposed to estimate the machine flux [10]. A general dynamic state estimation model for a permanent magnet synchronous generator is proposed in [11]. Another application of dynamic state estimation is converter health monitoring [12]. However, these existing methods either ignore the control dynamics or mix the digital control model with the physical inverter model in a single state space model, which cannot explicitly monitor the data flows between the two systems and is unable to detect anomalies in measurement signals or control signals.

In this paper, a novel cyber attack detection method based on dynamic state estimation is proposed for the secure operation of IBRs. In order to explicitly model the uncertainty in measurement and control data flows, the state-space models of the physical layer (inverter system) and the cyber layer (digital controller) are separately derived and then related by the input and output signals. Noting the symmetry between the two state spaces, a dual dynamic state estimation framework is proposed to track the internal states of both layers and detect anomalies in measurement and control data flows between the two layers. The key strength of the proposed method is that it not only detects false data with high reliability, but can accurately identify the source of false data, and distinguish between false data in measurement signals and control signals. This is a highly desirable feature as the closed-loop control makes false data affect both layers and difficult to trace.

II. Cyber-Physical Representation of IBR Models

To detect and distinguish between anomalies in measurement signals and control signals, the physical layer and cyber layer of IBRs are represented separately, such that these data flows between the two layers could be explicitly modeled and examined. The physical and cyber layers of the dual-stage grid following IBR connected to the grid are shown in Fig. 1.

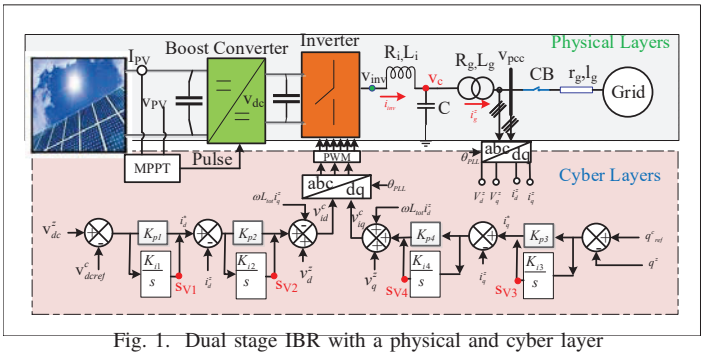

Fig. 1. Dual stage IBR with a physical and cyber layer

A. Physical state space representation of IBR

Typically, the physical layer of IBR has a few sensors that collect measurements and provide input to the digital controller. The differential equations characterizing the dynamics of the physical layer can be written as,

$$\begin{bmatrix} \dot{i}_{inv_{abc}} \\ \dot{v}_{c_{abc}} \\ \dot{i}_{g_{abc}} \end{bmatrix} = \begin{bmatrix} -\frac{R_i}{L_i} I_{3\times3} & -\frac{1}{L_i} I_{3\times3} & 0_{3\times3} \\ \frac{1}{C} I_{3\times3} & 0_{3\times3} & -\frac{1}{C} I_{3\times3} \\ 0_{3\times3} & \frac{1}{L_g} I_{3\times3} & -\frac{R_g}{L_g} I_{3\times3} \end{bmatrix} \begin{bmatrix} i_{inv_{abc}} \\ v_{c_{abc}} \\ i_{g_{abc}} \end{bmatrix} + \begin{bmatrix} \frac{1}{L_i} I_{3\times3} & 0_{3\times3} \\ 0_{3\times3} & 0_{3\times3} \\ 0_{3\times3} & -\frac{1}{L_g} I_{3\times3} \end{bmatrix} \begin{bmatrix} v_{inv_{abc}} \\ v_{pcc_{abc}} \end{bmatrix} \tag{1}$$

where $i_{inv_{abc}}$, $i_{g_{abc}}$ are inverter side current and grid side current; $v_{pcc_{abc}}$, $v_{inv_{abc}}$ and $v_{c_{abc}}$ are the point of common coupling voltage, voltage at inverter terminal and voltage across capacitor bank; L_i, R_i, L_g, R_g, and C are inverter side inductance and resistance, grid side inductance and resistance, and filter capacitance, respectively. Eq. (1) is referred to as state transition equations of the physical layer of IBR. The measurement signals are outputs of the physical layer, whose variables are determined by the states of the physical layer. The output equations can be written as,

$$i_{g_{abc}} = \begin{bmatrix} 0_{3\times3} & 0_{3\times3} & I_{3\times3} \end{bmatrix} \begin{bmatrix} i_{inv_{abc}} \\ v_{c_{abc}} \\ i_{g_{abc}} \end{bmatrix} \tag{2}$$

Hence, the state-space representation of the physical layer of dual stage grid following IBR in abc frame can be given as,

$$\dot{x}_{pl} = A_{pl} x_{pl} + B_{pl} u_{pl};\ y_{pl} = C_{pl} x_{pl} + D_{pl} u_{pl} \tag{3}$$

where the state variables, input signals, and output signals for physical layers of IBR are $x_{pl} = [i_{inv_{abc}}, v_{abc}, i_{g_{abc}}]^T$, $u_{pl} = [v_{inv_{abc}}, v_{pcc_{abc}}]^T$ and $y_{pl} = [i_{g_{abc}}]^T$, respectively; A_{pl} is the system matrix, B_{pl} is the input matrix, and C_{pl} is the output matrix and D_{pl} is the direct transmission matrix for the physical layer; the subscript pl denotes the physical layer.

B. Cyber state space representation of IBR

Taking the measurement signals from the physical layer as inputs, the controller performs digital computations to obtain control signals as outputs for inverter actuation to achieve specific operational objectives. Converting transfer functions into a state-space representation, the dynamics of the cyber layer of a dual-stage grid following IBR with Maximum Power Point Tracking (MPPT) in the dq frame can be written as,

$$\begin{bmatrix} \dot{s}_{v1} \\ \dot{s}_{v2} \\ \dot{s}_{v3} \\ \dot{s}_{v4} \end{bmatrix} = \begin{bmatrix} 0 & 0 & 0 & 0 \\ K_{i2} & 0 & 0 & 0 \\ 0 & 0 & 0 & 0 \\ 0 & 0 & K_{i4} & 0 \end{bmatrix} \begin{bmatrix} s_{v1} \\ s_{v2} \\ s_{v3} \\ s_{v4} \end{bmatrix} + \begin{bmatrix} K_{i1} & 0 & 0 & 0 \\ K_{p1}K_{i2} & -K_{i2} & 0 & 0 \\ 0 & 0 & K_{i3} & 0 \\ 0 & 0 & K_{p3}K_{i4} & -K_{i4} \end{bmatrix} \begin{bmatrix} v^z_{dc} - v^c_{dcref} \\ I^z_d \\ q^z - q^c_{ref} \\ i^z_q \end{bmatrix} \tag{4}$$

The control signals v^c_{id} and v^c_{iq} as outputs of the cyber layer are taken as the input of the physical layer, i.e., to generate the firing pulses for the inverter switches. The output equations of the cyber layer can be represented as,

$$\begin{bmatrix} v^c_{id} \\ v^c_{iq} \end{bmatrix} = \begin{bmatrix} K_{p2} & 1 & 0 & 0 \\ 0 & 0 & K_{p4} & 1 \end{bmatrix} \begin{bmatrix} s_{v1} \\ s_{v2} \\ s_{v3} \\ s_{v4} \end{bmatrix} + \begin{bmatrix} K_{p1}K_{p2} & -K_{p2} & 0 & -L_{tot}\omega \\ 0 & L_{tot}\omega & K_{p2}K_{p4} & -K_{p4} \end{bmatrix} \begin{bmatrix} v^z_{dc} - v^c_{dcref} \\ i^z_d \\ q^z - q^c_{ref} \\ i^z_q \end{bmatrix} \tag{5}$$

Hence, the state-space representation for cyber layers of IBR in a conventional dq frame can be given as,

$$\dot{x}_{cl} = A_{cl} x_{cl} + B_{cl} u_{cl};\ y_{cl} = C_{cl} x_{cl} + D_{cl} u_{cl} \tag{6}$$

where the state variables, input signals, and output signals for cyber layers of IBR are $x_{cl} = [s_{v1}, s_{v2}, s_{v3}, s_{v4}]^T$, $u_{cl} = [v^z_{dc} - v^c_{dcref}, i^z_d, q^z - q^z_{ref}, i^z_q]^T$ and $y_{pl} = [i_g]^T$; v_{dc}, i_d, i_q; q are PV side input voltage, grid side d, and q-axis currents and reactive power; $K_{p1} - K_{p2}$ and $K_{i1} - K_{i4}$ are proportional and integral gains of the controller as shown in Fig. 1; $L_{tot} = L_i + L_g$ and ω are total inductance and angular frequency; the superscripts z and c represent the measurement and control signal and subscript cl denotes the control layer.

III. Cyber Attack Detection Based on Dual Dynamic State Estimation

A. Overall framework

In this section, The dynamic state estimation framework is presented to track the internal cyber-physical states of IBR utilizing terminally available measurement and control signals. The cyber-physical representation of the IBR and the overal framework of the proposed method is shown in the Fig. 2. An interesting symmetry between the cyber and physical layers can be observed: the measurement signals are outputs of the physical layer but inputs to the cyber layer; on the contrary, the control signals are the outputs of the cyber layer but inputs to the physical layer. As the outputs of a layer are determined by the state transition and output models of this layer, it can be used to infer the internal states of this layer. Therefore, a dual dynamic state estimation framework is proposed: one

978-1-6654-6441-3/23/$31.00 ©2023 IEEE

estimator for tracking the states of the cyber layer based on the control signals, and another estimator tracking the states of the physical layer based on the measurement signals, respectively.

From Fig. 2, it is also clear that there are two possibilities of data falsification in the interaction between the two layers: falsification of measurement signals and falsification of control signals. As the outputs of a layer must follow the state transition and output models of the same layer, a hypothesis testing method is developed to detect inconsistencies due to data falsification and distinguish between anomalies in measurement signals and control signals.

B. Proposed algorithm

As the dynamic state estimators for the cyber and physical layers have dual structures, they can be described in a uniform fashion. To distinguish between the variables associated with cyber and physical layers, a subscript set $\Phi = \{pl, cl\}$ is used.

The KF is a widely used approach for tracking the state of linear dynamic systems [8]. As observed in (3) and (6), both the cyber and the physical layer of the IBR are linear when represented by the electromagnetic transient model. Therefore, for either layer, the discrete-time model by the forward Euler method can be rewritten as,

$$x_{\phi(k)} = F_\phi x_{\phi(k-1)} + B_\phi u_{\phi(k-1)} T_s + v_{\phi(k)}, \phi \in \Phi \quad (7)$$

$$y_{\phi(k)} = C_\phi x_{\phi(k)} + D_\phi u_{\phi(k)} + w_{\phi(k)}, \phi \in \Phi \quad (8)$$

where $F_\phi = (I + A_\phi)T_s$, T_s is sampling interval; v_{ϕ_k} and w_{ϕ_k} are white uncorrelated Gaussian noise with $v_{\phi_k} \sim (0, Q_{\phi_k})$ and $w_{\phi_k} \sim (0, R_{\phi_k})$. The following steps are used to estimate

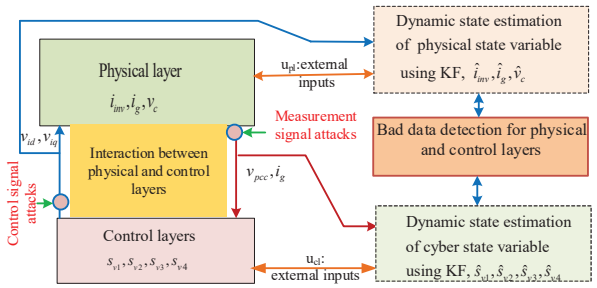

Fig. 2. Data flows between physical and cyber layers and the proposed method

the state variables of both the physical and the cyber layers. False data detection for both measurement signals and control signals is performed using the Largest Normalized Residual (LNR) hypothesis test [13] following state estimation in each time step. Initially, set $k = 0$.

1) For $\phi \in \Phi$, compute *a priori* state estimate and covariance matrix $\hat{x}_{\phi(k|k-1)} = F_\phi \hat{x}_{\phi(k-1|k-1)} + B_\phi u_{\phi(k-1)} T_s$, $P_{\phi(k|k-1)} = F_{\phi(k)} P_{\phi(k-1|k-1)} F^T_{\phi(k)} + Q_{\phi(k)}$.
2) For $\phi \in \Phi$, compute *a priori* measurement estimate and covariance matrix, and Kalman gain $\hat{y}_{\phi(k|k-1)} = C_\phi \hat{x}_{\phi(k|k-1)}) + D_\phi u_{\phi(k|k-1)}$, $S_{\phi(k)} = C_{\phi(k)} P_{\phi(k|k-1)} C^T_{\phi(k)} + R_{\phi(k)}$, $K_{\phi(k)} = P_{\phi(k|k-1)} C^T_{\phi(k)} S^{-1}_{\phi(k)}$.
3) For $\phi \in \Phi$, compute *a posteriori* state estimate and covariance matrix $\hat{x}_{\phi(k|k)} = \hat{x}_{\phi(k|k-1)} + K_{\phi(k)}(y_{\phi(k)} - \hat{y}_{\phi(k|k-1)})$, $P_{\phi(k|k)} = P_{\phi(k|k-1)} - K_{\phi(k)} C_{\phi(k)} P_{\phi(k|k-1)}$.
4) For $\phi \in \Phi$, compute Normalized Residual (NR) for all the output signals $res_{\phi(k)} = y_{\phi(k)} - C_{\phi(k)} \hat{x}_{\phi(k|k)}$, $\Omega_{\phi(k)} = R_{\phi(k)} - C_{\phi(k)} P_{\phi(k|k)} C^T_{\phi(k)}$, $res^N_{\phi(k)}(i) = \frac{|res_{\phi(k)}(i)|}{\sqrt{\Omega_{\phi(k)}(i,i)}}$, where i is the index of the output (measurement or control) signal.
5) Find the output signal with the LNR $(\hat{\phi}_{(k)}, \hat{i}_{(k)}) = argmax\{res^N_{\phi(k)}(i)\}$. If $res^N_{\hat{\phi}_{(k)}}(\hat{i}_{(k)}) > \zeta = 3.0$, false data is detected, go to Step 6), otherwise, no false data is detected, $k \leftarrow k+1$, go to Step 1).
6) If $\hat{\phi}_{(k)} = pl$, false measurement signal is detected, and $\hat{i}_{(k)}$ is the index of the measurement channel with false data; if $\hat{\phi}_{(k)} = cl$, false control signal is detected, and $\hat{i}_{(k)}$ is the index of the control channel with false data. Set false data flag $Flag_{\hat{\phi}_{(k)}}(\hat{i}_{(k)}) = 1$, and the false data flag of all the other measurement/control signals as 0. $k \leftarrow k+1$, go to Step 1).

Owing to the separate state-space modeling of the physical and cyber layers in Section II and the dual dynamic state estimation framework for the two layers, false data in measurement signals and in control signals can be distinguished from each other. The reason is discussed as follows. As measurement signals are outputs of the physical layer, the normalized residuals of measurement signals indicates the inconsistency between measurement signals and the physical layer model 3. Similarly, as control signals are outputs of the cyber layer, the normalized residuals of control signals cyber layer model 6. When a measurement signal or a control signal is falsified, although the disturbance will propagate across both layers due to the closed-loop structure, inconsistency will only be detected between the false signal and the model of the layer for which the false signal is the output. In addition, with the proven property of the LNR test [13], the LNR will correspond to the channel with the false data, and thus the source of the attack can be exactly identified.

IV. Simulation Results

To evaluate the performance of the proposed methods, the IEEE 13-node test feeder with the integration of five IBRs is considered as shown in Fig. 3. IBR1 and IBR2 are single-phase sources while IBR3-IBR5 are three-phase sources. The IBR1-IBR3 are grid following IBRs, whereas IBR4 and IBR5 have grid forming capability. Their ratings are given in Table I. The dynamic state estimator and cyber attack detector monitor IBR3 located at node 680, whose parameters are listed in Table I. The system frequency is 60Hz and the number of samples per cycle N_s is 120.

A. State tracking under solar irradiation change

The SPV-based IBR is highly intermittent in nature due to changes in solar irradiation patterns throughout the day of operation. The tracking performance of online dynamic state estimator for physical state variables $\hat{i}_{inv_{abc}}$, $\hat{v}_{c_{abc}}$, $\hat{i}_{g_{abc}}$

978-1-6654-6441-3/23/$31.00 ©2023 IEEE

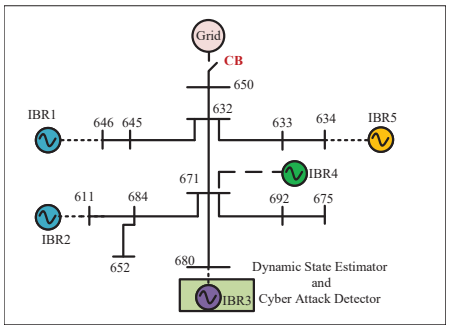

Fig. 3. IEEE 13 node test feeder with 5 IBRs

TABLE I
IBR RATINGS AND SPECIFIC PARAMETERS OF IBR3

IBRs	Rating kW	Voltage Level (V)	IBR3 Parameters					
IBR1	50	480, 1ϕ	L_i	0.06	K_{p1}	7	K_{i1}	800
IBR2	50	480, 1ϕ	L_g	0.14	K_{p2}	0.3	K_{i2}	20
IBR3	100	400, 3ϕ	R_i	0.003	K_{p3}	0.01	K_{i3}	0
IBR4	500	480, 3ϕ	R_g	0.002	K_{p4}	0.3	K_{i4}	20
IBR5	500	600, 3ϕ	C	0.003	N_s	120	ω	1

and cyber state variables $\hat{s}_{v1}, \hat{s}_{v2}, \hat{s}_{v3}, \hat{s}_{v4}$ for IBR3 (as in Fig. 3) is obtained for variation in solar irradiation from $(1000 \rightarrow 800 \rightarrow 500 \rightarrow 800 \rightarrow 1000) W/m^2$ at 0.4s, 0.5s, 0.6s and 0.7s, respectively as shown in Fig. 4. From Fig. 4 (a)-(c) and Fig. 5 (a)-(d), it can be observed that the actual trajectory and predicted trajectory of physical states and controller states are almost overlapping. As solar irradiation of solar PV changes, the grid current and inverter current of IBR3 is changing as can be observed from Fig. 4 (a) and (c). In contrast, the v_{c_a} remains the same in Fig. 4 (b) due to the grid following operation of IBR3. For ease of representation, only phase 'a' state variables are shown for physical layer. So, the proposed KF algorithm is able to rightly and accurately track states during dynamic operation of IBR3.

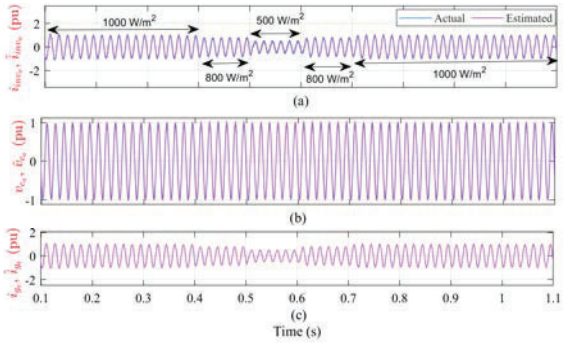

Fig. 4. (a) $\hat{i}_{inv_a}$ (b) $\hat{v}_{c_a}$ (c) $\hat{i}_{g_a}$ with change in solar irradiation of IBR3

B. State tracking under grid voltage change

IBRs are subjected to frequent terminal voltage fluctuations due to the change in grid operating conditions and faults. Hence, the tracking performance of the dynamic state estimator for the physical layer under a grid voltage change $v_{pcc} = 1 - 0.5$ pu between $0.4 - 0.7$s is tested, with results shown in Fig. 6. From Fig. 6 (b), it can be observed that $\hat{v}_{c_a}$ is dropped to 0.5 pu and i_{inv_a} and i_{g_a} is proportionally increased in Fig. 6 (a) and (d) due to MPPT operation of the

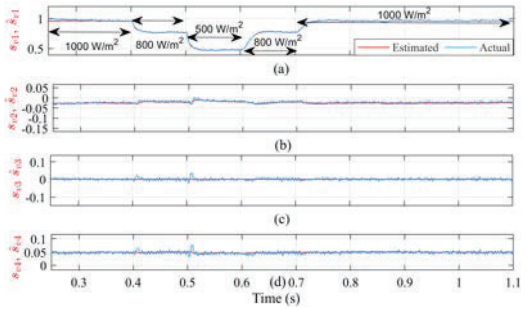

Fig. 5. (a) $\hat{s}_{v1}$ (b) $\hat{s}_{v2}$ (c) $\hat{s}_{v3}$ (d) $\hat{s}_{v4}$ with solar irradiation change of IBR3

grid following operation of IBR3. Similarly, the internal state variables for the cyber layer are obtained for $v_{pcc} = 1 - 0.9$pu during interval $0.4 - 0.7$s as shown in Fig. 7 (a)-(d). The state tracking results for physical and cyber layers are both accurate under the dynamic voltage conditions.

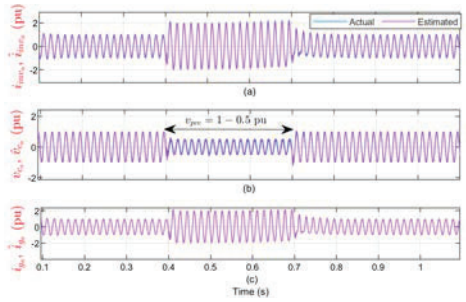

Fig. 6. (a) $\hat{i}_{inv_a}$ (b) $\hat{v}_{c_a}$ (c) $\hat{i}_{g_a}$ with change in grid voltage

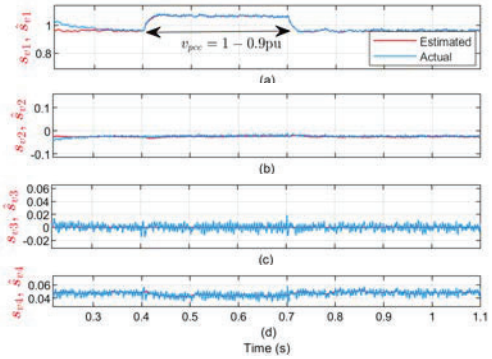

Fig. 7. (a) $\hat{s}_{v1}$ (b) $\hat{s}_{v2}$ (c) $\hat{s}_{v3}$ (d) $\hat{s}_{v4}$ with change in grid voltage

C. Cyber attack detection

The false data is injected into a measurement signal and a control signal at two different times during real-time operation of IBR3. Specifically, false measurement signal in phase 'a' of i_g is introduced at 0.4s as can be seen in the corrupted state variables shown in Fig. 8. Also, false control signal is injected in the d-axis voltage of IBR3 at 0.7s as can be seen in the corrupted state variables as shown in Fig 9. To identify it, the normalized residuals of measurement signals and control signals as shown in Fig. 10 (a) and Fig. 10 (c) are obtained through the proposed framework. $Flag_{pl}$ and $Flag_{cl}$ are shown in Fig. 10 (b) and Fig. 10 (d), which reflect the detection status of false data in measurement signals and control signals, respectively. Clearly, it can be stated that both false data

978-1-6654-6441-3/23/$31.00 ©2023 IEEE

are effectively detected by the proposed framework. More interestingly, by comparing the normalized residuals of all the signals, the proposed method also succesfully distinguish the source of false data. When the false measurement signal in phase 'a' of grid current i_g is introduced at 0.4s, only the normalized residual of $res^N_{i_{g_a}}$ exceeds ζ and generates the flag, while the normalized residuals of all other signals remain below the threshold; similarly, when the false control signal is injected in the d-axis voltage of IBR3 at 0.7s, only $res^N_{v_d}$ exceeds ζ and generates the flag. This shows that the proposed framework is able to trace the source of the attack and facilitates effective follow-up countermeasures.

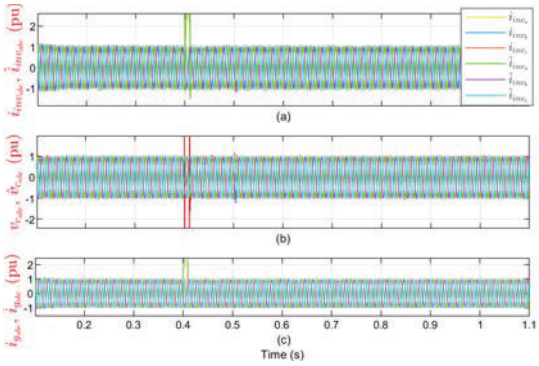

Fig. 8. (a) $\hat{i}_{inv_{abc}}$ (b) $\hat{v}_{abc}$ (c) $\hat{i}_{g_{abc}}$ with false data injection

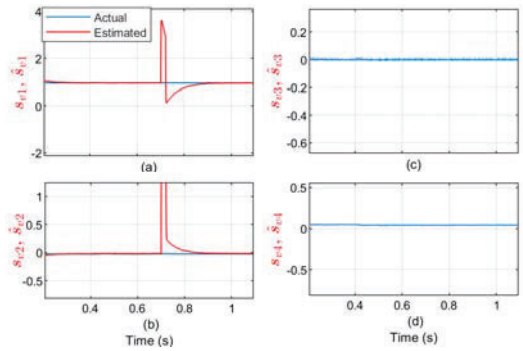

Fig. 9. (a) $\hat{s}_{v1}$ (b) $\hat{s}_{v2}$ (c) $\hat{s}_{v3}$ (d) $\hat{s}_{v4}$ with false data injection

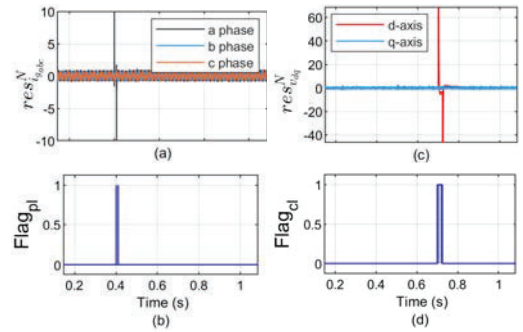

Fig. 10. (a) Normalized residuals of measurement signals, and (b) false data flags of measurement signals, (c) Normalized residuals of control signals and (d) false data flags of control signals

V. Conclusion

In this paper, an online dynamic state estimator and cyber attack detector are developed to track the cyber and physical state variables and attack events of IBRs. The mathematical state-space representations for physical and cyber layers are separately derived such that anomalies in measurement and control data flows between the two layers can be explicitly examined. Hypothesis testing is developed to check the consistency of measurement and control signals against the models of the physical and cyber layers, respectively. The proposed framework is demonstrated to be effective for tracking the internal states of an IBR under different transient conditions. Further, the developed approach is examined to have the capability to not only detect but also classify false data in measurement signals and control signals. The proposed approach could be helpful in enhancing the situational awareness and cyber security of IBRs under diverse operating scenarios.

Acknowledgement

This work is supported in part by Department of Navy award N00014-22-1-2001 issued by the Office of Naval Research and in part by Brookhaven National Laboratory Award #38456 issued by the U.S. Department of Energy.

References

[1] "Ieee guide for using ieee std 1547 for interconnection of energy storage distributed energy resources with electric power systems," *IEEE Std 1547.9-2022*, pp. 1–87, 2022.

[2] M. N. Alam, S. Chakrabarti, and A. Ghosh, "Networked microgrids: State-of-the-art and future perspectives," *IEEE Transactions on Industrial Informatics*, vol. 15, no. 3, pp. 1238–1250, 2019.

[3] N. D. Tuyen, N. S. Quan, V. B. Linh, V. Van Tuyen, and G. Fujita, "A comprehensive review of cybersecurity in inverter-based smart power system amid the boom of renewable energy," *IEEE Access*, vol. 10, pp. 35 846–35 875, 2022.

[4] I. Zografopoulos and C. Konstantinou, "Detection of malicious attacks in autonomous cyber-physical inverter-based microgrids," *IEEE Trans. Industrial Informatics*, vol. 18, no. 9, pp. 5815–5826, 2022.

[5] J. Zhao, A. Gomez Exposito, M. Netto, L. Mili, A. Abur, V. Terzija, I. Kamwa, B. Pal, A. K. Singh, J. Qi, Z. Huang, and A. P. S. Meliopoulos, "Power system dynamic state estimation: Motivations, definitions, methodologies, and future work," *IEEE Transactions on Power Systems*, vol. 34, no. 4, pp. 3188–3198, 2019.

[6] L. Dang, B. Chen, S. Wang, W. Ma, and P. Ren, "Robust power system state estimation with minimum error entropy unscented kalman filter," *IEEE Trans. Instrum. Meas.*, vol. 69, no. 11, pp. 8797–8808, 2020.

[7] A. Sharma, S. C. Srivastava, and S. Chakrabarti, "A cubature kalman filter based power system dynamic state estimator," *IEEE Trans. Instrum. Meas.*, vol. 66, no. 8, pp. 2036–2045, 2017.

[8] J. Zhao, M. Netto, and L. Mili, "A robust iterated extended kalman filter for power system dynamic state estimation," *IEEE Transactions on Power Systems*, vol. 32, no. 4, pp. 3205–3216, 2017.

[9] D. Sivadas and K. Vasudevan, "Stability analysis of three-loop control for three-phase voltage source inverter interfaced to the grid based on state variable estimation," *IEEE Transactions on Industry Applications*, vol. 54, no. 6, pp. 6508–6518, 2018.

[10] S. Yu, T. Fernando, K. Emami, and H. H.-C. Iu, "Dynamic state estimation based control strategy for dfig wind turbine connected to complex power systems," *IEEE Transactions on Power Systems*, vol. 32, no. 2, pp. 1272–1281, 2017.

[11] S. Song, P. Wu, Y. Lin, and Y. Chen, "A general dynamic state estimation framework for monitoring and control of permanent magnetic synchronous generators-based wind turbines," *IEEE Access*, vol. 9, pp. 72 228–72 238, 2021.

[12] K. Yue, Y. Liu, P. Zhao, B. Wang, M. Fu, and H. Wang, "Dynamic state estimation enabled health indicator for parametric fault detection in switching power converters," *IEEE Access*, vol. 9, pp. 33 224–33 234, 2021.

[13] Y. Lin and A. Abur, "A highly efficient bad data identification approach for very large scale power systems," *IEEE Transactions on Power Systems*, vol. 33, no. 6, pp. 5979–5989, 2018.